Atmospheric Trends and Lifetime of CH_3CCl_3 and Global OH Concentrations

R. G. Prinn, R. F. Weiss, B. R. Miller, J. Huang, F. N. Alyea, D. M. Cunnold, P. J. Fraser, D. E. Hartley, P. G. Simmonds

Determination of the atmospheric concentrations and lifetime of trichloroethane (CH_3CCl_3) is very important in the context of global change. This halocarbon is involved in depletion of ozone, and the hydroxyl radical (OH) concentrations determined from its lifetime provide estimates of the lifetimes of most other hydrogen-containing gases involved in the ozone layer and climate. Global measurements of trichloroethane indicate rising concentrations before and declining concentrations after late 1991. The lifetime of CH_3CCl_3 in the total atmosphere is 4.8 ± 0.3 years, which is substantially lower than previously estimated. The deduced hydroxyl radical concentration, which measures the atmosphere's oxidizing capability, shows little change from 1978 to 1994.

The hydroxyl radical (OH) is the major oxidizing chemical in the lower atmosphere and is responsible for the destruction of almost all hydrogen-containing gases involved in the chemistry of the ozone layer and the radiative forcing of climate. Because the global distribution of OH cannot presently be measured directly, it must be deduced from global measurements of atmospheric gases that are destroyed by OH, such as 1,1,1-trichloroethane (methyl chloroform, CH_3CCl_3). Trichloroethane is a purely anthropogenic volatile chemical and is restricted under the Montreal Protocol for the protection of the ozone layer.

Concentrations of CH_3CCl_3 have been measured at five globally distributed stations 4 to 12 times daily over the time period July 1978 to June 1994 in the Atmospheric Lifetime Experiment (ALE) and its successor, the Global Atmospheric Gases Experiment (GAGE) (*1–3*). When combined with industrial emissions estimates, measurements of CH_3CCl_3 can be used to determine its rate of destruction, and thus its lifetime, in the lower atmosphere. The global weighted-average lower atmospheric concentration and trend of OH is then derived from this lifetime (*1–4*). The derived OH concentrations can be used in turn to determine the lifetimes, and thus the potentials for stratospheric ozone depletion and global warming, of a wide range of chemicals (*5, 6*).

ALE-GAGE Measurements and Calibration

The ALE-GAGE stations are located in Ireland, Oregon, Barbados, Samoa, and Tasmania at coastal sites generally remote from industrial and urban sources. They are designed to measure accurately the tropospheric trends of trace gases whose lifetimes are long compared to global tropospheric mixing times (*7*). In ALE-GAGE, CH_3CCl_3 is analyzed in real time with microprocessor-controlled gas chromatographs that have silicone-coated packed columns and electron capture detectors (*1–3*). On-site calibration involves alternate analyses of dried outside air and dried gas from an on-site tank that is calibrated relative to working standards before and after its several-month use at the site (*8*).

Absolute calibration of the CH_3CCl_3 working standards, and hence of the measurements reported here, has been achieved recently using a "bootstrap" technique as a part of the GAGE follow-on, the Advanced Global Atmospheric Gases Experiment (AGAGE). In this technique, the accurately known absolute calibration for CO_2 is used together with accurate measurements of the N_2O to CO_2 and CH_3CCl_3 to N_2O ratios in standard gas mixtures to provide the final CH_3CCl_3 calibration (*9*). This calibration technique is superior to the microsyringe dilution method used to prepare the previous ALE-GAGE calibration (*3, 10*). The new method uses larger quantities of gas, is based on more accurately known mixtures with lower major to minor component ratios, and achieves a very high reproducibility of 0.1%. The method also includes the addition of 10 torr of H_2O in each CH_3CCl_3 dilution step to passivate electropolished stainless steel container surfaces, whereas the previous ALE-GAGE standards were prepared in similar containers using dry (<0.02 torr H_2O) "zero air" for dilution. We have confirmed that without this passivation, standard gas mixtures stored in these containers can be depleted significantly in CH_3CCl_3, thus leading to erroneously high reported atmospheric values. Analysis of four of the current ALE-GAGE working standards relative to the new CH_3CCl_3 AGAGE standard indicates that the CH_3CCl_3 absolute concentrations reported here are 0.818 of the previously reported ALE-GAGE concentrations (*3, 10*). This significant lowering of the absolute concentration means that our deduced CH_3CCl_3 lifetime, and OH concentrations and trends, differ considerably from previous estimates (*3*). The units for the CH_3CCl_3 measurements reported here are dry-air mole fractions expressed as parts in 10^{12} (ppt).

Monthly mean mole fractions χ and standard deviations σ computed from the approximately 120 to 360 measurements made each month in ALE-GAGE are shown in Fig. 1. These high-frequency measurements also resolve important short-term variations in trace gas concentrations within each month. These variations include pollution events at the mid-latitude stations in Ireland, Oregon, and Tasmania, involving sharp increases above background levels caused by regional circulation changes bringing air to the stations from nearby industrial regions (*3*). In contrast, at tropical stations, the large north-south gradients in CH_3CCl_3 concentration combined with changes in interhemispheric circulation lead to either increases or decreases when air originates from the north or south, respectively (*3*). We assume that the measurements, when averaged over time scales of a month or longer, are indicative of the region between the surface and the 500-mbar atmospheric height in the semihemisphere in which the station lies. Therefore, we specifically omitted periods of obvious local pollution at Ireland, Oregon, and Tasmania from the data used here to calculate χ and σ (*11*).

The latitudinal gradients in χ, the larger σ in the Northern compared to the Southern Hemisphere, and the annual cycles (Fig. 1) can be explained in terms of distances from sources (largely Northern Hemisphere mid-latitude), intensity and seasonality of the global circulation, and

---

R. G. Prinn and J. Huang are in the Department of Earth, Atmospheric, and Planetary Sciences, Massachusetts Institute of Technology, Building 54-1312, Cambridge, MA 02139-4307, USA. R. F. Weiss and B. R. Miller are with the Scripps Institution of Oceanography, University of California, La Jolla, CA 92093-0220, USA. F. N. Alyea, D. M. Cunnold, and D. E. Hartley are in the Department of Earth and Atmospheric Sciences, Georgia Institute of Technology, Atlanta, GA 30332, USA. P. J. Fraser is with the Commonwealth Scientific and Industrial Research Organization, Division of Atmospheric Research, Aspendale 3195, Victoria, Australia. P. G. Simmonds is in the Department of Biogeochemistry, University of Bristol, Bristol BS81TS, UK.

the variation in the major CH_3CCl_3 destruction reaction

$$OH + CH_3CCl_3 \rightarrow H_2O + CH_2CCl_3 \quad (1)$$

caused by the seasonal cycle (with summer maximum) in OH concentrations (*3*). Also, the Samoa data are sensitive to the El Niño–Southern Oscillation (ENSO). Specifically, the Samoa data is in phase with Tasmania during El Niño and out of phase otherwise, which is attributed to modulation of cross-equatorial transport by the ENSO (*3*).

Recent Decrease in CH_3CCl_3

The global measurements (Fig. 1) show that the concentration of CH_3CCl_3 has decreased significantly since 1991. This represents the first actual decrease in atmospheric concentration recorded for any halocarbon restricted under the Montreal Protocol on Substances that Deplete the Ozone Layer (*12*). The observed χ can be expressed as functions of time t (in years) by the empirical model

$$\chi(t) = a + bNP_1\left(\frac{t}{N} - 1\right) + \frac{1}{3}dN^2P_2\left(\frac{t}{N} - 1\right) + c\cos(2\pi t) + s\sin(2\pi t) \quad (2)$$

where the coefficients a, b, d, c, and s are determined optimally by weighting each χ by the inverse of σ^2. The P_i are Legendre polynomials of order i, and t is measured from the beginning of the $2N$-year interval of interest. To evaluate a, b, and d, we divided the data into two intervals: one with increasing χ (July 1978 to June 1990) and one with decreasing χ (July 1990 to June 1994). We evaluated c and s for the entire period, adding the polynomials P_3 and P_4 to Eq. 2 to better fit the full data set.

In Eq. 2, the average values over the $2N$ years for the rate of change of χ (trend) and the rate of change of the trend are given respectively by b/a and d/a. Combining Ireland and Oregon and averaging the trends at the resulting four stations, we then obtain "global" CH_3CCl_3 trends of 4.5 ± 0.1% per year (1978 to 1990) and −2.2 ± 0.4% per year (1990 to 1994). Similarly averaging the rates of change of trend, we obtain global rates of change in the CH_3CCl_3 trend of −0.3 ± 0.1% $year^{-2}$ (1978 to 1990) and −3.8 ± 0.8% $year^{-2}$ (1990 to 1994). Statistically significant annual cycles are seen in Ireland, Oregon, Barbados, and Tasmania, with amplitudes given by c/a and s/a (Table 1). An obvious annual cycle at Samoa, although not apparent from Table 1, is apparent if one divides the data into El Niño and non–El Niño periods (Fig. 1) (*3*).

Lifetime of CH_3CCl_3—Methods

The atmospheric lifetime τ of CH_3CCl_3 in an atmospheric region is the amount of CH_3CCl_3 in that region divided by its rate of destruction in (or removal from) the same region. To deduce τ values from χ and industrial emissions, we use an optimal estimation inversion technique (*13*). The technique produces a best guess of the unknowns (for example, τ) contained in a vector **y** and their errors contained in a matrix **C** by minimizing the squares of the deviations between the observed (vector **x**) and model-calculated (vector $\mathbf{x}_c$) values for χ or ln χ. The vector **y** is updated with each new month of data using

$$\Delta\mathbf{y} = \mathbf{CP}'[\mathbf{PCP}' + \mathbf{N}]^{-1}(\mathbf{x} - \mathbf{x}_c) \quad (3)$$

Here, **P** (and its transpose **P′**) is a matrix containing the partial derivatives of the elements of $\mathbf{x}_c$ with respect to the elements of **y**; **P** is computed as a function of time in the same atmospheric model used to predict $\mathbf{x}_c$ [we use the actual time series of these partial derivatives rather than a linear fit to the series as we have done previously (*3, 13*)]. The term **N** is a diagonal matrix whose nonzero elements are the variances (σ^2) in χ or ln χ at each site (Fig. 1). The matrix **C**, whose diagonal elements are the variances of the elements of **y**, is updated along with **y** using each month's observations (*13*). Estimates of **y** can be obtained with each station data set alone or all station data sets simultaneously.

The global atmospheric model used in the estimation technique is two-dimensional, consisting of eight lower atmospheric and four upper atmospheric boxes with horizontal divisions at 90°N, 30°N, 0°, 30°S, and 90°S and vertical divisions at 1000, 500, 200, and 0 mbar. The four lowest boxes (500 to 1000 mbar) provide predictions for comparison with the ALE-GAGE observations in the four semihemispheres, with the observations in Ireland and Oregon being combined for this purpose (*3*). Mean advective and eddy diffusive transports in the model are specified from meteorological observations and an optimal fit to global data for the chlorofluorocarbons $CFCl_3$ and CF_2Cl_2 (*13*). Because the model does not simulate intra-annual variations attributable to instrumental performance or many natural meteorological phenomena, we use the 12-month running mean calculations of χ from the model in $\mathbf{x}_c$. The model is then augmented by two empirical models that describe the spectrum of the differences between the observations and model predictions (*13*). Input into the model are estimates of CH_3CCl_3 emissions (Fig. 2), which are determined from global and regional sales and end-use data compiled by

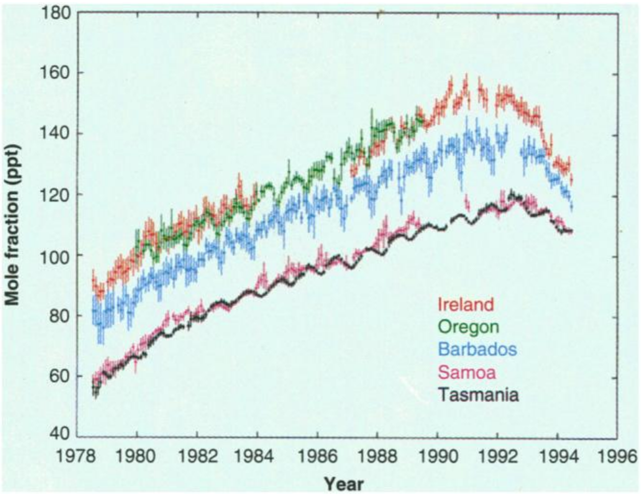

Fig. 1. Monthly mean mole fractions χ and standard deviations σ for the CH_3CCl_3 at ALE-GAGE stations. Where measurements from the ALE and GAGE instruments overlapped in time, the data were combined by weighting equally ALE and GAGE monthly means to determine χ and ALE and GAGE individual measurements to determine σ.

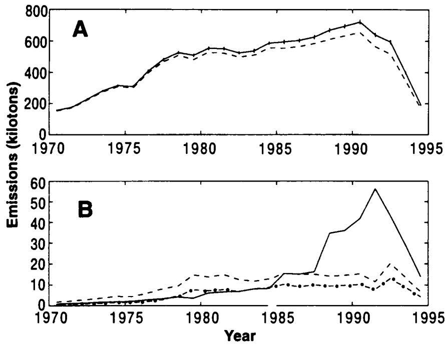

Fig. 2. Global and semihemispheric annual CH_3CCl_3 emissions computed from industry data for the period 1970 to 1994: (**A**) global (solid line) and 90°N to 30°N (dashed line) emissions; and (**B**) 30°N to 0° (solid line), 0° to 30°S (dash-dot line), and 30°S to 90°S (dashed line) emissions (*14, 15*). For data from before 1970, emissions were tabulated elsewhere (*15*). Units are 10^9 g (kilotons) per year. Uncertainty (1σ) in annual global emissions shown by the error bars is ±2.2% (random). Not shown is the ±1.5% (systematic) error.

Table 1. Average linear trend (*b/a*), rate of change in linear trend (*d/a*), and amplitude of annual cycle (*c/a* and *s/a*) obtained by optimally fitting Eq. 2 to the monthly observations (Fig. 1) at each ALE-GAGE station and the Ireland and Oregon stations combined, and also to the measurements of archived Cape Grim, Tasmania, air (*8*). Values for *b/a* and *d/a* are given for the two periods July 1978 to June 1990 and July 1990 to June 1994, whereas values for *c/a* and *s/a* are for the entire data set. Uncertainties are 1σ.

Station	July 1978 to June 1990		July 1990 to June 1994		July 1978 to June 1994	
	b/a (% year^{-1})	*d/a* (% year^{-2})	*b/a* (% year^{-1})	*d/a* (% year^{-2})	*c/a* (%)	*s/a* (%)
Ireland	3.93 ± 0.07	−0.09 ± 0.06	−4.69 ± 0.32	−4.56 ± 0.55	0.64 ± 0.31	−0.86 ± 0.31
Oregon	3.86 ± 0.10	−0.09 ± 0.07			−0.89 ± 0.33	−1.51 ± 0.33
Ireland-Oregon	3.98 ± 0.07	−0.28 ± 0.04			−0.03 ± 0.28	−1.24 ± 0.28
Barbados	4.18 ± 0.06	−0.19 ± 0.04	−2.89 ± 0.24	−3.65 ± 0.49	0.62 ± 0.23	−1.44 ± 0.23
Samoa	4.81 ± 0.13	−0.32 ± 0.09	−0.64 ± 0.69	−3.08 ± 1.23	−0.22 ± 0.46	−0.21 ± 0.46
Tasmania	4.90 ± 0.06	−0.39 ± 0.05	−0.53 ± 0.25	−3.78 ± 0.46	0.87 ± 0.24	1.37 ± 0.24
Air archive	4.97 ± 0.11	−0.18 ± 0.09	−1.15 ± 0.26	−2.84 ± 0.50		

the industry (*14–16*). Uncertainty in these annual semihemispheric emissions is estimated to be ±2.2% (random error) and ±1.5% (systematic error) (*15*). Because our results are dependent on the trend in (and the magnitude of) the annual emissions, we also considered emissions for 1978 to 1994, which possess the maximum and minimum trends in this time period consistent with their 2σ (±4.4%) random errors (*3*).

Initial estimates of the τ resulting from chemical destruction in each of the 12 atmospheric boxes and loss to the ocean from the four lowest atmospheric boxes are obtained from global circulation and chemistry models and ocean observations (*17*). The τ in the four upper atmospheric boxes and the τ from loss to the ocean in the four lowest atmospheric boxes were kept constant during each run of the inversion technique. The values of $1/\tau$ resulting from reaction with OH in the eight lower atmospheric boxes are dimensionless and were multiplied by a single estimated coefficient α (which is the inverse of the lower atmospheric lifetime resulting from reaction with OH), which provided an optimal fit between observed and modeled CH_3CCl_3 mole fractions and trends. By augmenting α to account for the ocean sink, we obtain the inverse of the lower atmospheric lifetime α^* (*17*). We also estimated either the linear trend β in α or α^* (caused by a trend in OH concentrations) or the dimensionless calibration coefficient (which multiplies all the χ values). Initial values for the unknowns (for example, α and β, or α and γ contained in **y**) and their uncertainties (square roots of the corresponding diagonal elements of **C**) are taken as $\alpha = \alpha \pm \alpha$, $\ln \gamma = 0.0 \pm 0.25$, and $\beta/\alpha = 0.0 \pm 0.1$ year^{-1}, with the initial uncertainties being large to avoid biasing the final estimates.

Lifetime of CH_3CCl_3—Results

We determine the unknowns using five methods that optimally fit different features of the data and have different sources of possible error (*3*, *13*). Our first method (trend), which focused on fitting the measured fractional trends $d\ln\chi/dt$, was insensitive to absolute calibration errors but sensitive to emission trends and modeling uncertainties. Figure 3 shows the convergence toward an estimate of the lower atmospheric inverse lifetime α^*, and Table 2 summarizes the results. The estimated lifetime, assumed industrial emissions, and model transports lead to a satisfactory fit to the observations, including the magnitude and phase lag of

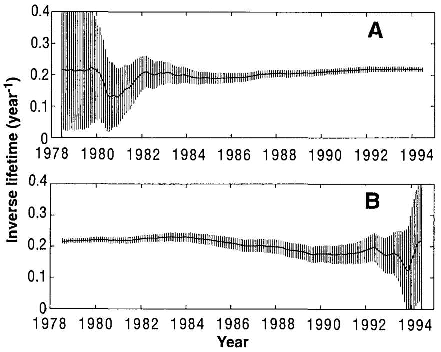

Fig. 3. Inverse lower atmospheric lifetime (α^*) and 1σ uncertainty (error bars) estimated by applying Eq. 3 in the trend method (**A**) in the last forward run in time and (**B**) in a backward run. The next-to-last forward run and the backward run yielded the same estimates as the last forward run (as demanded for convergence and expected from the recursive Eq. 3). Before each run, the **P** matrix time series was recomputed with the estimate of the tropospheric lifetime from the preceding run. Each run began with the estimates for the vector **y** (α^*, γ) from the end of the preceding run, but the initial uncertainties in **y** were always reset to those used in the initial run.

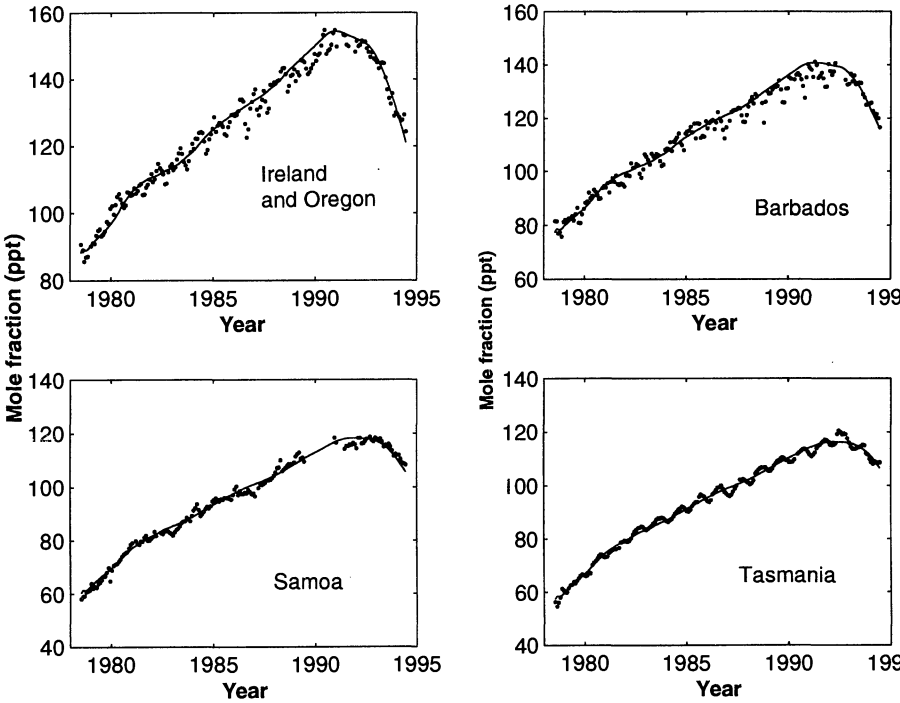

Fig. 4. Observed χ in each semihemisphere (dots) compared to the predicted χ values from the four lowest boxes of the 12-box model (continuous lines) in the final forward run in the trend method.

the change in sign in the trend as one goes from north to south (Fig. 4). The trend method also provided an estimate of $\gamma = 0.983$, which is well within the assumed ±5% uncertainty in calibration (*9*).

A second method (variable lifetime) estimated the time average of α (or α^*) and linear trend β in α (or α^*), keeping γ constant (unity). The time-averaged α^* calculated by this method, which is sensitive to emission, calibration, and modeling uncertainty, is shown in Table 2. In the third and fourth methods (content methods), the inverse lifetimes were obtained by optimally fitting the observed annual changes in χ. The content method was applied to the entire 16 years of data and also to each year of data alone followed by averaging the inverse lifetimes from each year (annualized content method). The variable lifetime method and the two content methods are sensitive to emission, absolute calibration, and modeling errors (the latter involving assumed model lifetimes, lifetime gradients, and exchange times). The fifth method focuses on optimally fitting the measured concentrations at individual stations relative to the global average (gradient method). The gradient method is sensitive to errors in the distribution of emissions with latitude and to certain modeling uncertainties (interhemispheric transport rates, upper atmospheric lifetime, and lower atmospheric OH latitudinal gradients).

We see good agreement between the lifetimes deduced by the trend and content methods (Table 2) in contrast to our previously published estimates based on the old absolute calibration (*3*). Also, the best estimate (Table 2) of the lower atmospheric lifetime ($1/\alpha^* = 4.6 \pm 0.3$ years) is significantly lower than our previous best estimate of $5.7^{+0.7}_{-0.6}$ years (*3*). Repeating the calculations in Table 2 with the old calibration yielded a trend-method lifetime of 4.6 years (identical with the Table 2 value), variable lifetime and content and annualized content lifetimes of 6.0, 6.4, and 6.1 years, respectively (in very poor agreement with the Table 2 values), and a best estimate lifetime of 5.7 years (essentially identical with our previous best estimate, which was based on 12 rather than 16 years of data). These agreements are expected because the trend method is not sensitive to absolute calibration, whereas the variable lifetime and two content methods are.

Trend and Concentrations of OH

The trend in α or α^* (and thus in the weighted average OH concentration) deduced by both the variable lifetime and annualized content methods is 0.0 ± 0.2% per year. The uncertainty here includes uncertainty in the emissions, emissions trend, absolute calibration, and model parameters (lower atmosphere to upper atmosphere exchange time and upper atmospheric lifetimes). The inferred trend in the CH_3CCl_3 inverse lifetime and OH concentrations is sensitive to absolute calibration (*3*). Using the old calibration yields a trend by the variable lifetime and annualized content methods that is essentially the same value reported in (*3*), namely, 1.0 ± 0.8% per year. The differences between our new values and those reported previously for the CH_3CCl_3 lifetime and the trend in OH result, therefore, largely from the change in absolute calibration.

Table 2. Estimates of lower atmospheric inverse lifetime α^* and lifetime $1/\alpha^*$ for CH_3CCl_3 derived by five methods and data from all sites. Using data only from single sites, we find the trend lifetimes are 4.5, 4.6, 4.9, and 4.8 years for Ireland-Oregon, Barbados, Samoa, and Tasmania, respectively. The content lifetimes are 4.5 years for each site. The quoted errors include emission, modeling, and calibration errors, which are added to observational uncertainty (that is, *N*), and are determined by repeating the runs for each method with the maximum and minimum of emissions (*15*), trends in emissions (*15*), absolute calibration (*9*), upper atmospheric lifetimes (*17*), equator-to-pole gradients in lower atmospheric lifetimes resulting from OH (*17*), and lower atmospheric-to-upper atmospheric and interhemispheric exchange times (*13*), to determine the errors caused by each. The square root of the sum of the squares of these errors then provides the quoted uncertainties. The "best estimate" is obtained by summing the trend, variable lifetime, content, annualized content, and gradient inverse lifetimes with equal (20%) weight. Similar results, including the same best estimate lifetime, are obtained with independently assessed emissions (*16*). Uncertainties are 1σ.

Case	α^* (year^{-1})	$1/\alpha^*$ (years)
1. Trend lifetime with emission trend and model uncertainties included	0.217 ± 0.025	$4.6^{+0.6}_{-0.5}$
2. Variable lifetime with emission, calibration, emission trend, and model uncertainties included	0.222 ± 0.017	$4.5^{+0.4}_{-0.3}$
3. Content lifetime with emission, calibration, and model uncertainties included	0.222 ± 0.017	$4.5^{+0.4}_{-0.3}$
4. Annualized content lifetime with emission, calibration, emission trend, and model uncertainties included	0.223 ± 0.018	$4.5^{+0.4}_{-0.3}$
5. Gradient lifetime with emission and modeling uncertainties included	0.208 ± 0.034	$4.8^{+0.9}_{-0.7}$
6. Best estimate		
Standard error	0.218 ± 0.009	$4.6^{+0.2}_{-0.2}$
Basic (full range) error	$0.218^{+0.024}_{-0.044}$	$4.6^{+1.2}_{-0.5}$

To convert the deduced CH_3CCl_3 lower atmospheric inverse lifetimes in each lower atmospheric box in the model to average OH concentrations, we subtract the loss rate due to the ocean in the four lowest lower atmospheric boxes to yield CH_3CCl_3 lifetimes τ_i in each box due to OH alone (*17*). Using the rate equation for Reaction 1 between OH and CH_3CCl_3, these τ_i are related to the average OH concentrations $[OH]_i$ in each box i by

$$1/\tau_i = k_i(T_i)[\mathrm{OH}]_i \tag{4}$$

where k_i is the temperature-dependent rate constant in box i for the reaction of OH with CH_3CCl_3 and T_i is the average temperature in box i (*18*, *19*). These procedures can also be applied to the entire lower atmosphere and yield a CH_3CCl_3 lower atmospheric lifetime ($1/\alpha$) due to OH of 4.9 ± 0.3 years (compared to $1/\alpha^* = 4.6 \pm 0.3$ years including the ocean sink) and a temperature and atmospheric density-weighted average OH concentration of $(9.7 \pm 0.6) \times 10^5$ radicals cm^{-3} (the OH uncertainty does not include errors in rate constants).

The lower atmospheric (500 to 1000 mbar) lifetime τ_x of any other gas "x" due to reaction with OH can be deduced from the above results by

$$\frac{1}{\tau_x} = \sum_{i=1}^{8} \frac{f_{xi} k_{xi}(T_i)}{\tau_i k_i(T_i)} \tag{5}$$

where f_{xi} is the fraction of the total lower atmospheric mass of gas x in box i, and $k_{xi}(T_i)$ is its temperature-dependent rate constant (*18*, *19*). Carrying out the summation in Eq. 5 over all 12 boxes yields the total atmospheric (0 to 1000 mbar) lifetime. For CH_3CCl_3 itself, the total atmospheric lifetime is 4.8 ± 0.3 years. For the radiatively and chemically important gas methane, Eq. 5 yields a lower atmospheric lifetime due to OH of 8.0 ± 0.5 years and a total atmospheric lifetime of 8.9 ± 0.6 years with model-calculated f_{xi} and methane stratospheric lifetime (*20*). Similarly, for the hydrochlorofluorocarbon CHF_2Cl (HCFC-22), the tropospheric and total atmospheric lifetimes are 10.5 ± 0.7 and 11.5 ± 0.7 years, respectively.

Summary

Atmospheric concentration of the volatile anthropogenic chemical CH_3CCl_3, which was steadily increasing at 4.5 ± 0.1% per year until mid-1990, has subsequently decreased at a rate of 2.2 ± 0.4% per year (all stated uncertainties are 1σ). This recent rapid decrease is consistent with its short lifetime and recent industrial emission reductions. The observed decreases began in early 1991 in the Northern Hemisphere and in mid-1992 in the Southern Hemisphere, reflecting the predominantly Northern Hemispheric emissions of this industrial chemical and the approximately 1-year interhemispheric exchange time. The measurements, combined with industrial emissions, were used in an inverse method to deduce a globally averaged CH_3CCl_3 lower atmospheric lifetime (200 to 1000 mbar) of 4.6 ± 0.3 years and a total atmospheric lifetime (0 to 1000 mbar) of 4.8 ± 0.3 years. Assuming a lifetime for loss of CH_3CCl_3 to the oceans of 85 years, we deduced a global weighted-average lower atmospheric OH concentration of $(9.7 \pm 0.6) \times 10^5$ radicals cm^{-3}. The rate of change of this OH concentration is 0.0 ± 0.2% per year, implying that the oxidation capability of the lower atmosphere has not changed significantly from 1978 to 1994. Our conclusions concerning the OH concentrations and trend depend on the accuracy of the industrial emission estimates and our new absolute calibration. For methane (CH_4), these OH concentrations imply lower atmospheric and total atmospheric lifetimes of 8.0 ± 0.5 and 8.9 ± 0.6 years, respectively. The deduced lifetimes for CH_3CCl_3 and CH_4 are substantially less and the deduced OH concentrations substantially more than previous estimates (*3, 5, 6*). This lowers substantially the potential of these two gases (and most other hydrogen-containing gases) for affecting the ozone layer and climate compared to previous estimates (*5, 6*). The constancy of the lower atmospheric OH concentration implies that increasing OH levels cannot serve as an explanation for the observed dramatic decreases in CH_4 trends and CO concentrations in recent years (*21*). Also, increases in lower atmospheric OH levels, expected as a result of recent accelerated total ozone depletion (*22*), must, at least at low latitudes, be offset by other factors (despite the fact that the above CO decreases would tend to lower the rate of OH destruction).

REFERENCES AND NOTES

1. R. G. Prinn *et al.*, *J. Geophys. Res.* **88**, 8415 (1983).
2. R. G. Prinn *et al.*, *Science* **238**, 945 (1987).
3. R. G. Prinn *et al.*, *J. Geophys. Res.* **97**, 2445 (1992).
4. H. Singh, *Geophys. Res. Lett.* **4**, 453 (1977); J. E. Lovelock, *Nature* **267**, 32 (1977); Y. Makide and F. S. Rowland, *Proc. Natl. Acad. Sci. U.S.A.* **78**, 5933 (1981); P. Bloomfield *et al.*, in (*6*), chap. 3.
5. D. L. Albritton and R. T. Watson, *Global Ozone Research and Monitoring Project Report 25* (World Meteorological Organization, Geneva, 1991); M. J. Kurylo *et al.*, *NASA Ref. Publ. 1337* (National Aeronautics and Space Administration, Washington, DC, 1994); J. T. Houghton *et al.*, Eds., Intergovernmental Panel on Climate Change (IPCC), *Climate Change 1992* (Cambridge Univ. Press, Cambridge, 1992); *Radiative Forcing of Climate Change* (Cambridge Univ. Press, Cambridge, 1994).
6. J. A. Kaye *et al.*, Eds., *NASA Ref. Publ. 1339* (National Aeronautics and Space Administration, Washington, DC, 1994).
7. The stations are located in Cape Grim, Tasmania (41°S, 145°E); Point Matatula, American Samoa (14°S, 171°W); Ragged Point, Barbados (13°N, 59°W); Cape Meares, Oregon, USA (45°N, 124°W, 1980 to 1989 only); Adrigole, Ireland (52°N, 10°W, 1978 to 1983 only); and Mace Head, Ireland (53°N, 10°W, 1987 to present).
8. The on-site calibration procedure assumes a linear relation between instrument response and mixing ratio. An investigation of the on-site instruments and the instruments used to analyze the on-site calibration tanks in 1988 and 1989 showed that nonlinearity may contribute an uncertainty to the quoted CH_3CCl_3 trends of 0.0 ± 0.2% per year, which was comparable to or less than the uncertainty in these trends resulting from true atmospheric variability and may also have simply represented the accuracy with which samples were prepared for the nonlinearity tests (*3*). A new detector installed in the Tasmanian instrument in 1992 showed nonlinearity in 1993 still lying within the 1988 to 1989 range. The error resulting from drift in the working standards was assessed by intercomparing a set of tanks. For seven tanks over the 1978 to 1989 time period, this intercomparison indicated a possible drift error of about 0.02 ± 0.20% per year (*3*); for three tanks for 1990 onward, this indicated a possible error of 0.1 ± 0.2% per year. These possible errors are again generally small compared to the observed trends. Finally, as a measure of the combined effects of nonlinearity, stability, and on-site calibration tank preparation errors, a collection of tanks filled a few times annually beginning in 1978 at Cape Grim and stored were recently analyzed [P. J. Fraser *et al.*, in *Baseline 89*, S. L. Wilson and J. L. Gras, Eds. (Commonwealth Scientific and Industrial Research Organization and Bureau of Meteorology, Melbourne, Australia, 1991), pp. 16–29; I. A. Weeks *et al.*, in *Baseline 90*, S. L. Wilson and J. L. Gras, Eds. (Commonwealth Scientific and Industrial Research Organization and Bureau of Meteorology, Melbourne, Australia, 1992), pp. 16–23]. This analysis yielded the trends given in Table 1, which are not significantly different from those measured in ALE-GAGE at Tasmania, also shown in Table 1. The GAGE experiment is now being replaced by AGAGE, whose station instruments avoid the nonlinearity errors using automated on-site nonlinearity diagnosis and correction.
9. Our CH_3CCl_3 mole fractions use the AGAGE Scripps Institution of Oceanography (SIO) 1993 calibration scale. The SIO "bootstrap" calibration method combines the absolute calibration for CO_2 [C. D. Keeling *et al.*, *Tellus* **28**, 538 (1976)] with separate calibrations of the ratios of N_2O to CO_2 [R. F. Weiss, C. D. Keeling, H. Craig, *J. Geophys. Res.* **86**, 7197 (1981)] and of halocarbons to N_2O [J. L. Bullister and R. F Weiss, *Deep-Sea Res.* **35**, 839 (1988)]. The application of the method to obtain the AGAGE SIO-1993 calibrations of the halocarbons CCl_3F and CCl_2F_2 has already been described (*23*). A mixture of halocarbons and N_2O in approximately their current atmospheric ratios is prepared gravimetrically from the pure components. Approximately 0.4 ml of this mixture is injected through a high-pressure gas chromatography sampling valve into a 35-liter high-pressure internally electropolished stainless steel tank, together with 40 atm of halocarbon-free and N_2O-free N_2 and O_2 "zero air" and 10 torr of H_2O to aid surface passivation [A. Yokohata, Y. Makide, T. Tominaga, *Bull. Chem. Soc. Jpn.* **58**, 1308 (1985)]. The resulting halocarbon concentrations are determined from the prepared gravimetric halocarbon to N_2O ratios, multiplied by the measured N_2O concentration in the mixture [R. F. Weiss, *J. Chromatogr. Sci.* **19**, 611 (1981)]. For CH_3CCl_3, the precision of absolute standard preparation from four standards is ±0.1%, and the precision of the transfer of these AGAGE absolute standards to four ALE-GAGE working standards is ±0.2%. At this preliminary stage, the accuracy of the absolute standards is estimated conservatively as ±2%. To take into account possible transfer errors and past nonlinearity errors (*8*), we generously increase the uncertainty in absolute calibration for our calculations to ±5%. The complete set of AGAGE absolute calibrations is still in progress.
10. M. A. K. Khalil and R. A. Rasmussen, *Chemosphere* **13**, 789 (1984).
11. Polluted air also contains gases that could interfere with our measurements. The entire ALE-GAGE database, including pollution events, is accessible at the Carbon Dioxide Information Analysis Center at the U.S. Department of Energy, Oak Ridge National Laboratory, through Internet (FTP to cdiac.esd.ornl.gov).
12. United Nations Environment Programme, 1985 Vienna Convention for the Protection of the Ozone Layer, 1987 Montreal Protocol, 1990 London Amendment, 1992 Copenhagen Amendment.
13. For the inversion technique, see D. M. Cunnold *et al.*, *J. Geophys. Res.* **88**, 8379 (1983) and D. M. Cunnold and R. G. Prinn, *ibid.* **96**, 17391 (1991). For the 12-box model, see R. G. Prinn *et al.*, *ibid.* **95**, 18369 (1990). The troposphere-to-stratosphere exchange time in the 12-box model is significant in our analysis and is 2 ± 1 years on the basis of results from atmospheric models for CH_3CCl_3 (*17*) and chlorofluorocarbons (*23*).
14. P. M. Midgley, *Atmos. Environ.* **23**, 2663 (1989).
15. Global and semihemispheric emissions and their uncertainties for 1951 to 1969 are taken from (*2*). Global emissions and uncertainties for 1970 to 1979 are based on industry production and sales data (*3*). Percentage 1970 to 1980 emissions in each semihemisphere given in (*3*) have been adjusted slightly (0.5 to 0.9% subtracted from 30°N to 0° and added to 30° to 90°N) to agree with revised 1980 values cited below. The 1981 to 1993 emissions are computed from 1980 to 1993 industrial data [from (*14*), updated in (*24*)] by first multiplying them by 0.99 to account for manufacturing losses, incineration, and incarceration, and then assuming time delays between sales and emission of 0.25 year for "immediate release" uses (solvents, for example), 0.75 year for "medium release" uses, and 1.25 years for "slow release" (stockpiling) uses. Percentage 1980 to 1993 emissions in each semihemisphere are assumed to be the same as the semihemispheric sales reported by Midgley (*14, 24*) because the "immediate release" category makes up about 96% of total sales. Emissions for 1994 were obtained by a quadratic polynomial extrapolation of the 1990 to 1993 emissions. The emissions so defined agree very well with emissions estimated for 1971 to 1990 by D. A. Fisher *et al.* [in (*6*), chap. 2], but neither our emissions nor theirs include unreported production, estimated by them to be 1.5 ± 1.5% of reported production. Hence, we increase the above annual emissions by 1.5% and assume a systematic error of ±1.5% in these adjusted emissions.
16. We also considered emissions that have been recently estimated independently by P. M. Midgley and A. McCulloch [*Atmos. Environ.*, in press]. These differ only in small details from those in Fig. 2.
17. For the two-dimensional models, see A. R. Douglass *et al.*, *J. Geophys. Res.* **94**, 9862 (1989); C. H. Jackman *et al.*, *ibid.* **95**, 7417 (1990); M. K. W. Ko *et al.*, *ibid.* **96**, 7547 (1991). For the three-dimensional model, see A. Golombek and R. G. Prinn (*25*); *Nature* **344**, 47 (1990). For all three models, see also M. K. W. Ko *et al.*, in (*6*), chap. 5. The α values calculated in these three models are first each normalized to unity and then the $1/\tau$ in these models for each of 12 regions (corresponding to the 12 boxes of the model used in our inverse technique) are averaged. The 1σ standard deviations in these averages are used to define the maximum and minimum upper atmospheric $1/\tau$ and (after multiplying by $\sqrt{2}/2$) the maximum and minimum equator-to-pole gradients in the lower atmospheric $1/\tau$. The $1/\tau$ in the four upper atmospheric boxes are 0.060 ± 0.041, 0.264 ± 0.129, 0.254 ± 0.127, and 0.065 ± 0.040 $year^{-1}$ from south to north, respectively. The dimensionless $1/\tau$ resulting from OH in the eight lower atmospheric boxes (south to north, bottom to top) are 0.55 ± 0.05, 2.21 ± 0.58, 1.69 ± 0.08, 0.44 ± 0.15, 0.29 ± 0.09, 0.96 ± 0.39, 0.84 ± 0.43, and 0.26 ± 0.09.

These dimensionless values, multiplied by our final estimate of $\alpha = 0.204 \pm 0.013$ year^{-1}, provide the actual values ($1/\tau_i$). The latter $1/\tau_i$ in the four lowest boxes are augmented to include an ocean sink with global lifetime (global amount of CH_3CCl_3 divided by global rate of removal by ocean) of 85 years [J. H. Butler *et al.*, *J. Geophys. Res.* **96**, 22347 (1991)] distributed in proportion to the ocean area in each box (ignoring any possible minor temperature effects).

18. The deduced OH concentrations (10^5 radical cm^{-3}) in the eight lower atmospheric boxes are (from south to north and bottom to top) 5.5, 15.9, 12.2, 4.3, 6.4, 15.8, 13.7, and 5.7. See W. B. DeMore *et al.*, *NASA Jet Propulsion Laboratory Publ. 94-26* (1994) for rate constants used here.
19. Going from south to north and bottom to top, the appropriate average temperatures T_i in the eight lower atmospheric boxes are 278, 293, 293, 278, 241, 253, 253, and 241 K, respectively. A simplified version of Eq. 5 regards the whole troposphere as a single box, in which case the appropriate average tropospheric temperature is 277 K [M. J. Prather and C. M. Spivakovsky, *J. Geophys. Res.* **95**, 18723 (1990)] and, from our results, the lower atmospheric CH_3CCl_3 lifetime to use is $\alpha^{-1} = 4.9 \pm 0.3$ years.
20. The model of Golombek and Prinn (*25*) has total atmospheric lifetimes resulting from upper atmospheric destruction alone of 112 and 131 years for CH_4 and $CHClF_2$, respectively. Total lifetime uncertainty includes stratospheric destruction uncertainty for CH_3CCl_3 (*17*), but not for CH_4 and $CHClF_2$.
21. E. J. Dlugokencky *et al.*, *Geophys. Res. Lett.* **21**, 45 (1994); P. C. Novelli, K. A. Masarie, P. P. Tans, P. M. Lang, *Science* **263**, 1587 (1994).
22. S. Madronich and C. Granier, *Geophys. Res. Lett.* **19**, 465 (1992).
23. D. M. Cunnold *et al.*, *J. Geophys. Res.* **99**, 1107 (1994).
24. P. M. Midgley, personal communication (letter dated 6 July 1994).
25. A. Golombek and R. G. Prinn, *J. Geophys. Res.* **91**, 3985 (1986).

26. This research was supported by NASA grants NAGW-732 and NAGW-474 (R.G.P. and J.H.), NAGW-732 (F.N.A., D.M.C., D.E.H.), and NAGW-2034 (R.F.W. and B.R.M.); National Oceanic and Atmospheric Administration (NOAA) contract NA85-RAC05103 (P.G.S.); Chemical Manufacturers Association contracts FC-85-567 (P.G.S.) and FC-87-640 (P.J.F.); United Kingdom Department of Environment contract PECD 7/10/54 (P.G.S.); Commonwealth Scientific and Industrial Research Organization (P.J.F.); and Bureau of Meteorology, Melbourne, Victoria, Australia (P.J.F.). Valuable local support at the ALE-GAGE stations was provided by D. Brown (Mace Head, Ireland), P. Sealey (Ragged Point, Barbados), C. Brunson and M. Winey (Cape Matatula, Samoa), and L. Porter (Cape Grim, Tasmania). We thank R. A. Rasmussen and A. J. Crawford for their contributions to the ALE-GAGE experiment, including operation of the Cape Meares, Oregon, and Cape Matatula, Samoa, stations before 1989. Finally, we thank M. Ko, N. D. Sze, D. Weisenstein, C. H. Jackman, and A. R. Douglass for kindly providing results from their two-dimensional models used in our analysis.

RESEARCH ARTICLE

Protein Folding Intermediates: Native-State Hydrogen Exchange

Yawen Bai, Tobin R. Sosnick, Leland Mayne,
S. Walter Englander*

The hydrogen exchange behavior of native cytochrome c in low concentrations of denaturant reveals a sequence of metastable, partially unfolded forms that occupy free energy levels reaching up to the fully unfolded state. The step from one form to another is accomplished by the unfolding of one or more cooperative units of structure. The cooperative units are entire omega loops or mutually stabilizing pairs of whole helices and loops. The partially unfolded forms detected by hydrogen exchange appear to represent the major intermediates in the reversible, dynamic unfolding reactions that occur even at native conditions and thus may define the major pathway for cytochrome c folding.

Under native conditions, a small fraction of any population of protein molecules occupies each possible higher energy, partially unfolded state, including even the fully unfolded state, as described by the Boltzmann distribution. The study of these partially unfolded forms (intermediates) may illuminate the fundamental cooperative nature of protein structure and define the unfolding and refolding pathways of a protein even though the intermediates are normally invisible to measurement. The energy levels and therefore the occupation of these conformationally excited states can be manipulated by denaturants and temperature. Hydrogen exchange experiments can then determine the hydrogens exposed in each higher energy form, their rates of exchange with solvent, and their sensitivity to the perturbant. From this we can infer, respectively, the structure, the free energy, and the surface exposure of each protein form.

Results for cytochrome c reveal a small sequence of distinct partially unfolded forms with progressively increasing free energy and degree of unfolding. These appear to represent the major intermediates in the unfolding and refolding pathways of cytochrome c.

Hydrogen exchange theory. Exchangeable amide hydrogens (NH) that are involved in hydrogen-bonded structure can exchange with solvent hydrogens only when they are transiently exposed to solvent in some kind of closed to open reaction (*1–3*), as indicated in Eq. 1.

$$\text{NH(closed)} \overset{K_{op}}{\rightleftharpoons} \text{NH(open)} \xrightarrow{k_{ch}} \text{exchanged} \qquad (1)$$

In the almost universally observed limiting case, referred to as EX2 (for bimolecular exchange) (*1*), the structural opening reaction enters the rate expression as a preequilibrium step. The exchange rate of any hydrogen, k_{ex}, is then determined by its chemical exchange rate in the open form, k_{ch}, multiplied by the equilibrium opening constant, K_{op} (Eq. 2).

$$k_{ex} = K_{op} k_{ch} \qquad (2)$$

Since the free peptide rate, k_{ch}, is known from model studies (*4–6*), the measurement of k_{ex} leads to K_{op} (Eq. 2) and the free energy for the dominant opening reaction, ΔG_{op} (Eq. 3).

$$\Delta G_{op} = -RT \ln K_{op} = -RT \ln (k_{ex}/k_{ch}) \qquad (3)$$

where R is the gas constant and T is the absolute temperature. Any structurally blocked hydrogen may be exposed to exchange by many different unfolding reactions with differing K_{op} values. The opening with the greatest K_{op} (smallest ΔG_{op}) will dominate the hydrogen exchange behavior.

The hydrogen exchange behavior measured here is in the EX2 limit. This is shown by the agreement between the ΔG_{op} values calculated for various hydrogens with disparate k_{ch} values (Figs. 1 to 5). In the alternative EX1 case (*1*) (monomolecular exchange) the exchange rate is independent of k_{ch}, and therefore correcting the different hydrogens for their k_{ch} differences would make ΔG_{op} values controlled by the same opening appear to be disparate.

Opening reactions that may determine protein hydrogen exchange rates have been discussed in terms of the breakage of single hydrogen bonds (*7*), the concerted local unfolding of small protein segments (*3, 8*), and whole molecule unfolding (*9–11*). Here we deal with a new class of large but still subglobal unfolding reactions. All these cases, although different structurally, are governed by the same mathematical relations (Eqs. 2 and 3).

The authors are at The Johnson Research Foundation, Department of Biochemistry and Biophysics, School of Medicine, University of Pennsylvania, Philadelphia, PA 19104-6059, USA.

*To whom correspondence should be addressed.